5106 *Biochemistry* **2009,** *48,* 5106–5120
DOI: 10.1021/bi802245u

BIOCHEMISTRY
including biophysical chemistry & molecular biology
Article

Structural Basis for Dimerization of the BNIP3 Transmembrane Domain[†,‡]

Endah S. Sulistijo[§] and Kevin R. MacKenzie*

Department of Biochemistry and Cell Biology, Rice University, 6100 Main Street, Houston, Texas 77005[§] Current address: Department of Biochemistry, Vanderbilt University, Nashville, TN 37232-8725.

Received December 9, 2008; Revised Manuscript Received May 3, 2009

ABSTRACT: Mutagenesis data suggest that BNIP3 transmembrane domain dimerization depends critically on hydrogen bonding between His 173 and Ser 172, but a recent structural analysis indicates that these residues adopt multiple conformations and are not always hydrogen bonded. We show that in dodecylphosphocholine micelles the structure of the BNIP3 transmembrane domain is modulated by phospholipids and that appropriate reconstitution and lipid titration yield a single set of peptide resonances. NMR structure determination reveals a symmetric dimer in which all interfacial residues, including His 173 and Ser 172, are well-defined. Small residues Ala 176, Gly 180, and Gly 184 allow close approach of essentially ideal helices in a geometry that supports intermonomer hydrogen bond formation between the side chains of His 173 and Ser 172. Bulky residues Ile 177 and Ile 181 pack against small residues of the opposite monomer, and favorable polar backbone−backbone contacts at the interface likely include noncanonical Cα−H·O=C hydrogen bonds from Gly 180 to Ile 177. Modeling mutations into the structure shows that most deleterious hydrophobic substitutions eliminate the His−Ser hydrogen bond or introduce an intermonomer clash, indicating critical roles for sterics and hydrogen bonding in the sequence dependence of dimerization. Substitutions at most noninterfacial positions do not alter dimerization, but the disruptive effects of substitutions at Ile 183 cannot be rationalized in terms of peptide−peptide contacts and therefore may indicate a role for peptide−detergent or peptide−lipid interactions at this position.

The lateral association of single transmembrane domains (TMDs)[1] within a bilayer to form higher-order structures provides opportunities to study structural and energetic contributions to membrane protein folding (reviewed in ref (*1*)). Isolated single spanning TMDs are likely to adopt canonical helical geometry and rotameric side chain orientations because these conformations correspond to local free energy minima. The structure of the glycophorin A TMD dimer (*2*) revealed that the interfacial side chains adopt backbone-dependent rotamer conformations (*3*) that correspond to local energy minima for each residue within a helical monomer while also providing favorable backbone−backbone and backbone−side chain interactions in the context of the dimer. This example supports a strict interpretation of the two-stage model of membrane protein folding proposed by Popot and Engelman (*4*): a hydrophobic sequence directed to membranes will form an α-helix, and such helices can associate laterally through favorable enthalpic interactions to form a bundle. Residues important for glycophorin A dimerization (*5*, *6*) map to the dimer interface (*2*), and the qualitative effects of mutations can be rationalized in terms of the structure (*7*). The contributions of interfacial residues to the thermodynamics of glycophorin A dimerization in detergents can be complex (*8*−*10*) but are largely consistent with the structure and with measurements taken in membranes (*11*). Although structural measurements in bilayers indicate slight conformational changes compared to detergents (*12*), the glycophorin A system adopts a stable dimeric structure that serves as an icon for thinking about interactions between single spans.

Despite the significance of the glycophorin A system, a rigid application of the two-stage model is not appropriate for all interacting TMDs. Some sequences directed to membranes require lateral interactions to achieve full helicity (*13*) or even to be fully incorporated into bilayers (*14*). Folding of an integral membrane protein can drive side chain or backbone conformations away from local energy minima: many polytopic proteins contain significantly kinked transmembrane helices or re-entrant loops. Populating a single low-energy structure is clearly not desirable for the many membrane channels, pumps, and transporters that undergo functionally important conformational changes within the membrane. Lateral associations of single spanning TMDs into helical bundles can exhibit complexity similar to that of polytopic membrane proteins: detailed

[†]This work was supported by NIH R01 GM-067850 and by Robert T. Welch Foundation grant C-1513.
[‡]Data deposited as Protein Data Bank entries 2ka1 and 2ka2 and BMRB accession number 16012.
*To whom correspondence should be addressed. E-mail: mev@rice.edu. Phone: (713) 348-2228. Fax: (713) 348-5154.
[1]Abbreviations: TMD, transmembrane domain; DPC, dodecylphosphocholine; DPPC, dipalmitoylphosphatidylcholine; DHPC, dihexanoylphosphatidylcholine; DMPC, dimyristoylphosphatidylcholine; DPPA, dipalmitoylphosphatidic acid; rmsd, root-mean-square deviation.

 Published on Web 05/05/2009

structures of the M2 channel from influenza virus (*15*, *16*) provide a basis for evaluating functionally relevant lipid-dependent conformational states (*17*) and pH-dependent conformational changes (*18*, *19*) of the channel. The combination of thermodynamic investigations of the sequence dependence of oligomerization and activity (*20*) and high-resolution structures (*16*) has identified trade-offs among stability, function, and drug resistance in this clinically important molecule (*21*). As structures of oligomeric TMD systems become available (*22*−*24*), quantitative analysis of the energetics of lateral association (reviewed in ref (*25*)) should help our general understanding of the folding energetics of globular, polytopic helical bundle membrane proteins. A sufficiently detailed understanding of individual oligomeric TMD systems could also lead to inhibitors of protein−protein interactions with roles as therapeutic agents (*26*).

BNIP3, a "BH3-only" member of the Bcl-2 superfamily of proteins, is induced in response to hypoxia (*27*) and is a central player in the hypoxia-induced death of both normal and malignant cells (*28*). We have shown that the TMD of BNIP3 forms dimers in detergent and in membranes (*29*), and we have investigated the sequence dependence of this homodimerization in detergent (*30*). The residues critical to dimerization include a "glycine zipper" motif (*31*) (Ala 176, Gly 180, and Gly 184) and two residues with polar side chains, Ser 172 and His 173. Our mutational analysis showed that the side chain oxygen of Ser 172 is essential for dimerization: mutations to Ala or Gly abolish the interaction (*30*). On the basis of this and additional mutagenesis data, we proposed that the two polar residues form intermonomer side chain−side chain hydrogen bonds that contribute to dimer stability (*30*).

Hydrogen bonds make important contributions to membrane protein stability because dipolar interactions are minimally screened in a low-dielectric environment (*32*). Additionally, poor partitioning of water into the apolar membrane core leaves few alternate hydrogen bonding partners for any membrane-buried polar groups. The formation of hydrogen bonds between main chain atoms enables polypeptides to partition into and span bilayers (*33*, *34*), explaining the predominance of β-barrels and α-helices as membrane protein architectures (*35*). Modified proteins that lack particular main chain hydrogen bonding partners are difficult to generate, precluding direct measurement of the contributions of individual main chain hydrogen bonds to protein stability, but side chain hydrogen bonding partners are readily altered by mutagenesis. Protein design experiments have shown that a single polar residue can drive strong association of an otherwise hydrophobic helix in membranes and in detergents (*36*, *37*), with each monomer stabilized within the oligomer by 1−2 kcal mol^{-1} (*38*). In contrast, eliminating an intermonomer side chain−side chain hydrogen bond has only modest effects on dimerization of a β-barrel membrane protein (*39*). Eliminating single side chain hydrogen bonds destabilizes bacteriorhodopsin by as much as 1.7 kcal mol^{-1}, but such changes often only minimally perturb protein stability, with the average effect being rather modest (0.6 kcal mol^{-1}) (*40*). Understanding why some side chain−side chain hydrogen bonds make significant energetic contributions to membrane protein stability while others do not is a challenge for membrane structural biology and biophysics.

Thermodynamic measurements in the BNIP3 system could extend this analysis, but the His−Ser hydrogen bonds inferred from our mutagenesis study have not been clearly demonstrated structurally. DeGrado and colleagues used a computational approach to predict the structure of the BNIP3 interface; in their model, one His−Ser pair forms an intermonomer hydrogen bond but the other does not (*41*). Arseniev and colleagues published a family of solution NMR structures of the BNIP3 TMD peptide dimer solubilized in DHPC/DMPC bicelles in which His 173 and Ser 172 are usually close enough to hydrogen bond; however, the His side chain is not well-defined across all family members, and some structures are not consistent with intermonomer hydrogen bond formation (*42*). These authors observed heterogeneities in the chemical shifts of residues Ser 172 and Ala 176 that they indicate are consistent with slow exchange between different conformers; they conclude that the BNIP3 TMD peptide assumes multiple states, particularly in the region of these interfacial residues (*42*). Here, we present a solution NMR study of the BNIP3 TMD in the detergent dodecylphosphocholine (DPC). We show that chemical shift heterogeneities seen in our detergent-solubilized preparations can be altered or eliminated by titrating phospholipids into the sample. Using a sample that exhibits a single set of resonances throughout, we determine the structure of the BNIP3 TMD peptide dimer and identify a single, well-defined conformation for the dimer interface that includes a symmetric pair of His−Ser side chain−side chain hydrogen bonds. We also present a structure-based analysis of how hydrophobic mutations could affect dimerization of this membrane span.

EXPERIMENTAL PROCEDURES

BNIP3 TMD Peptide Production, Purification, and NMR Sample Preparation. We used the pT7SN/BNIP3 plasmid construct (*29*, *30*) for high-level expression of a SN−BNIP3TM fusion protein in *Escherichia coli* to obtain large amounts of the BNIP3 TMD by trypsin cleavage (*29*, *43*). The construct employed has a stop codon after residue 188 because this truncation did not affect dimerization (*30*) and also has residue 152 deleted because adjacent lysine residues (Lys 152 and Lys 153) generated a mixture of trypsin fragments. This deletion does not affect dimerization of the SN−BNIP3TM fusion protein or heterodimerization of the fusion protein with the peptide, and trypsin cleavage of the TR188/ΔLys152 construct generates a single 35-amino acid BNIP3 TMD peptide with the native sequence GGIFSAEFLKVFLPSLLLSHLLAIGLGIYIGRRLT.

Expression of the [U-^{13}C,^{15}N]SN−BNIP3TM Fusion Protein. *E. coli* BL21(DE3) cells were transformed with the pT7SN/BNIP3TM vector, and we created glycerol stocks by inoculating colonies in 5 mL of LB medium supplemented with 50 μg/mL carbenicillin, shaking them at 37 °C until they reached an OD_{600} of ∼0.2, bringing aliquots of culture to 15% (v/v) glycerol, and storing them at −80 °C. Both labeled and unlabeled proteins were expressed by growing cell cultures in M9 minimal medium; for expression of the labeled protein, the M9 medium was prepared with [^{13}C]glucose and $^{15}NH_4Cl$. Expression of the SN−BNIP3TM fusion protein was started by inoculating from a glycerol stock into 5 mL of M9 minimal medium supplemented with 50 μg/mL carbenicillin and 100 μL of LB. The culture was shaken overnight at 37 °C, diluted 1:200 in 1 L of fresh M9 minimal medium supplemented with 50 μg/mL carbenicillin, and shaken at 37 °C until it reached an OD_{600} of ∼1.0, when protein expression was induced via addition of 0.5 mM IPTG. After being shaken for an additional 3 h at 37 °C, the cells were harvested by centrifugation at 10000*g* for 10 min.

Extraction and Purification of the SN−BNIP3TM Fusion Protein. The cell pellet was resuspended in a 1:20 culture volume of lysis buffer [20 mM Tris-HCl and 2 mM EDTA (pH 8.0)] and subjected to three rounds of freezing and thawing followed by probe sonication to lyse the cells. Next, 10 mM $CaCl_2$ and 0.1 mg/mL hen egg white lysozyme were added, and the whole cell lysate was incubated on ice for 30 min to allow cleavage of the chromosomal DNA by SNase. The whole cell lysate was then centrifuged at 12000*g* for 20 min; the supernatant was removed by decantation and discarded, and the pellet was subjected to successive washes in (1) lysis buffer containing 1 M ammonium acetate and (2) lysis buffer containing 2% (w/v) Thesit (Fluka). During each wash, the resuspended pellet was probe sonicated and separated from the soluble fraction by centrifugation at 12000*g* for 20 min. The SN−BNIP3TM fusion protein was extracted from the twice-washed pellet by sonication with lysis buffer containing both 1 M ammonium acetate and 2% (w/v) Thesit and recovered from the supernatant after centrifugation at 12000*g* for 20 min. This supernatant was dialyzed extensively against lysis buffer with 100 mM ammonium acetate and 0.2% (w/v) Thesit to lower both ammonium acetate and Thesit concentrations, clarified by centrifugation at 12000*g* for 30 min, and passed over a DE52 column. The DE52 flow-through was bound to a CM52 column, and the fusion protein was eluted with lysis buffer containing 400 mM ammonium acetate and 0.2% (w/v) Thesit.

Generation and Purification of BNIP3 TMD Peptide. BNIP3 TM peptide was isolated from the SN−BNIP3TM fusion protein by cleavage with 0.1 mg/mL trypsin for at least 8 h. The digestion product was dialyzed against lysis buffer to remove SN fragments, excess Thesit, and ammonium acetate. The cleaved, dialyzed material was lyophilized to dryness, and Thesit was extracted by washing with hexane and with a hexane/*n*-butanol/acetic acid mixture (6:1:0.1), two or three rounds each. The remaining peptide was purified with reversed-phase HPLC using a phenyl column and a gradient of acetonitrile and isopropyl alcohol (3:2) in water with 0.1% (v/v) trifluoroacetic acid. The identity and purity of the BNIP3 TM peptide collected from HPLC was confirmed by MALDI-TOF.

NMR Sample Preparation. The sample for NMR structure determination was reconstituted with a final composition of 0.4 mM [U-^{13}C,^{15}N]BNIP3 TMD peptide and 0.6 mM unlabeled BNIP3 TMD peptide in 128 mM d_{38}-dodecylphosphocholine (DPC, Cambridge Isotope Laboratories) and 10 mM sodium phosphate (pH 5.1) in a volume of 350 μL. Dried, HPLC-purified BNIP3 TMD peptide was resuspended and completely dissolved in hexafluoroisopropanol and water (1:1), and an amount of detergent that would correspond to the final conditions was added dropwise as a concentrated (~10%) aqueous solution to the peptide solution with mixing. Water was added to the sample dropwise until the detergent formed micelles (bubbles that form upon agitation persist rather than immediately popping), usually at hexafluoroisopropanol:water ratios between 1:2 and 1:4; care was taken to ensure that neither phase separation nor precipitation occurred in this step. The mixture was frozen rapidly in liquid nitrogen and lyophilized at low pressure and with the lyophilization bell jar chilled to prevent the peptide/detergent mixture from thawing, which can lead to peptide aggregation. To completely drive off organic solvents, samples were dissolved in water, frozen in liquid nitrogen, and lyophilized again. The completely dried peptide/detergent sample has a white, fluffy appearance (does not look greasy) and instantly dissolves in 200 μL of water. After the sample was brought to the target volume, including 10% (v/v) D_2O, NaH_2PO_4 was added to a final concentration of 10 mM and the pH was adjusted to 5.1 without correcting for the deuterium isotope effect. An internal standard [3-(trimethylsilyl)propionic acid-d_4, sodium salt] was added to a final concentration of 0.1 mM.

Lipid Preparation. Aliquots of 1,2-dipalmitoyl-*sn*-glycero-3-phosphocholine (DPPC-d_{75}, Avanti) or 1,2-dipalmitoyl-*sn*-glycero-3-phosphate (DPPA-d_{62}, Avanti) from chloroform stocks were dried by blowing argon or nitrogen gas, followed by vacuum drying. The dried lipids were resuspended in a 5% (w/v) aqueous d_{38}-DPC solution with 10% (v/v) D_2O. To ensure incorporation of the lipids in the DPC micelles, the mixture was incubated at 50 °C and sonicated briefly in a water bath sonicator. Addition of these aqueous lipid mixtures to reconstituted peptide/detergent NMR samples (described in the previous paragraph) diluted the peptide without changing the concentration of detergent. Optimal spectra were obtained after the addition of 10 mM d_{75}-dipalmitoylphosphatidylcholine (DPPC); some spectra were also recorded after addition of d_{62}-dipalmitoylphosphatidic acid (DPPA). Unlabeled samples of lipids were prepared in the same manner and mixed with detergent-reconstituted doubly labeled peptide to generate samples used to search for intermolecular lipid−protein NOEs.

NMR Experiments. All spectra were recorded at 40 °C on Varian Inova spectrometers equipped with triple-resonance cold probes; most data were acquired at 800 MHz, but pulse sequences using ^{13}C isotropic mixing were acquired at 600 MHz. The quality of BNIP3 TMD peptide samples was evaluated using two-dimensional (2D) ^{1}H−^{15}N heteronuclear single-quantum coherence (HSQC) spectra and ^{1}H−^{13}C HSQC spectra (methyl region). Standard triple-resonance sequences were implemented using the BioPack suite. NOE mixing times of 50 ms were used, except for a half-filtered NOESY-CN-HSQC spectrum (*44*), which was acquired with a 60 ms mixing time. ^3J couplings were calculated from intensities in a three-dimensional (3D) HNHA spectrum and in 2D spin−echo difference spectra (*45*, *46*). Spectra were processed using NMRPipe (*47*) and analyzed using Sparky (T. D. Goddard and D. G. Kneller, *SPARKY 3*, University of California, San Francisco).

Assignments. Backbone resonance assignments for optimized BNIP3 TMD peptide samples were obtained using standard triple-resonance experiments (HNCA, CBCACONNH, and HNCO). These spectra (and all 2D correlation spectra) reveal only a single set of resonances, consistent with a single symmetric conformation for each monomer within the dimer. Aliphatic side chain chemical shifts were assigned using 3D H(C)CH-COSY and (H)CCH-TOCSY spectra, and most aromatic chemical shifts were assigned using HBCBCGCDHD and HBCBCGCDCEHE spectra (*48*) in combination with 2D HSQC spectra; through-space correlations from a 3D NOESY-HSQC spectrum optimized for aromatic protons were used to assign the Phe Hζ and Cζ resonances. This spectrum also yielded NOE distance restraints resolved in two aromatic chemical shift dimensions, which helped resolve some chemical shift ambiguities in NOE assignments. The aromatic Cγ shifts were recorded using a modification of the HBCBCGCDHD experiment (*48*). ^3J couplings were calculated from intensities in a 3D HNHA spectrum and in 2D spin−echo difference spectra (*45*, *46*).

Restraints and Structure Calculation of the BNIP3 TMD Peptide Dimer. We calculated the structure of the BNIP3 TMD peptide dimer using ARIA version 1.2 (*49*) and

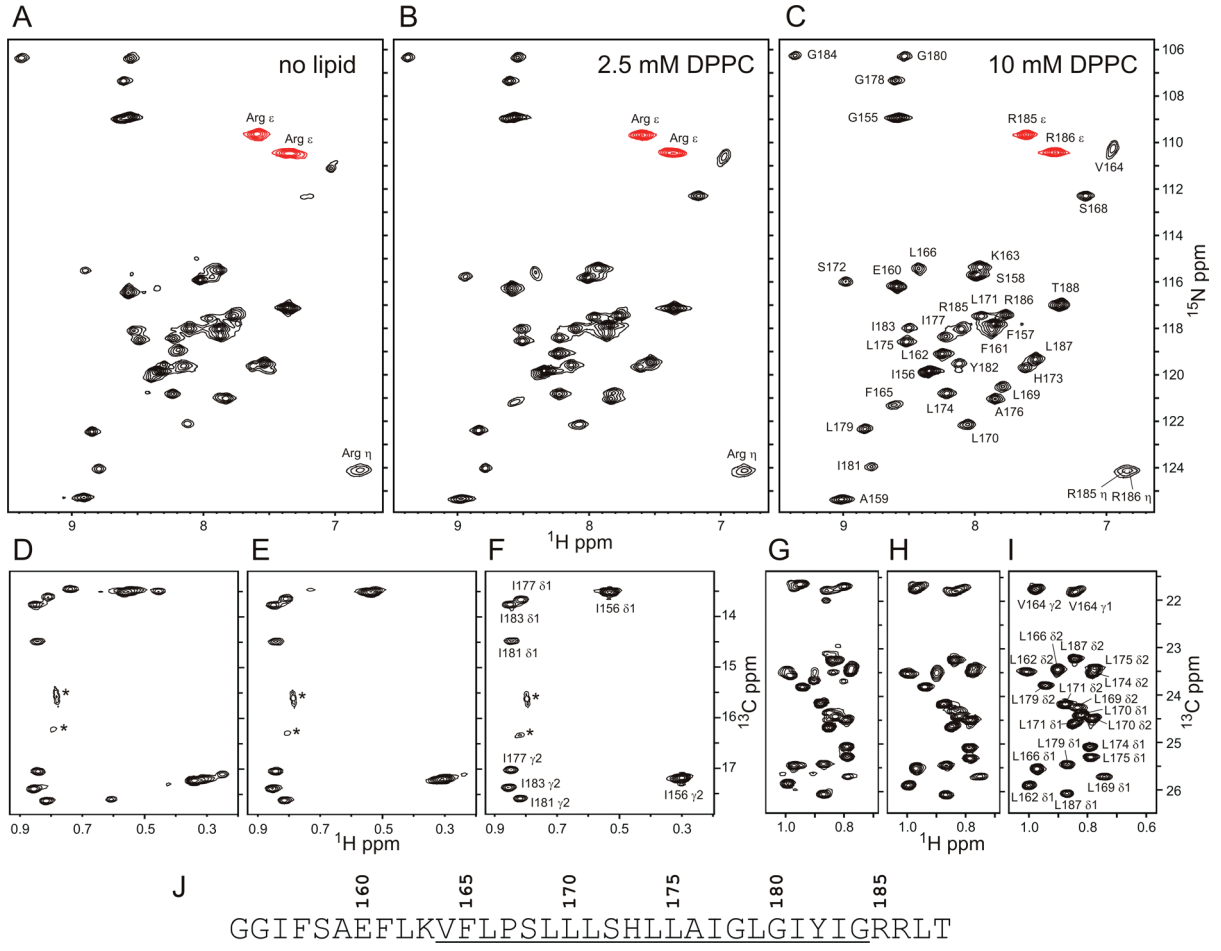

FIGURE 1: Effect of DPPC on spectra of the BNIP3 TMD peptide in DPC micelles. 2D heteronuclear correlation spectra acquired at 800 MHz, 40 °C, 5% DPC, and pH 5.1 show how backbone amides (A−C), isoleucine methyls (D−F), and valine/leucine methyls (G−I) of a single BNIP3 TMD peptide sample are affected by lipid titration. Panels A, D, and G were acquired with no lipid present; panels B, E, and H are spectra of the same sample acquired after addition of 2.5 mM DPPC dissolved in DPC, and panels C, F, and I were acquired after the concentration of the added DPPC had been increased to 10 mM. The concentration of DPC in the aliquots of added lipid was 5%, meaning that lipid addition dilutes the peptide slightly but does not alter the concentration of the detergent. Peaks marked with an asterisk in panels D−F are residual ^{1}H in deuterated DPC or DPPC. The sequence of the BNIP3 peptide is given in panel J.

CNS (*50*). The experimental restraints used in this calculation include ambiguous and intermonomer NOE distance restraints, backbone and side chain torsion angle restraints, and hydrogen bond restraints for the α-helical regions. Each NOE peak from our 3D ^{13}C- or ^{15}N-edited NOESY HSQC spectra could correspond to an intramonomer contact, an intermonomer contact, or a combination thereof. This ambiguity was explicitly identified in the ARIA input files, and each NOE was converted into a pair of ambiguous restraints: one restraint from proton 1 monomer A to proton 2 monomer A or B and another from proton 1 monomer B to proton 2 monomer A or B. Each exclusively intermonomer NOE from a half-filtered 3D CN-NOESY-HSQC spectrum (*44*) was converted to a pair of unambiguous restraints: one restraint from proton 1 monomer A to proton 2 monomer B and another from proton 1 monomer B to proton 2 monomer A. Slight modifications to ARIA 1.2 and CNS code were made to allow ARIA 1.2 to handle a homodimeric complex (code available in the Ph.D. Thesis of E. S. Sulistijo through The University of Michigan, Ann Arbor, MI). Intermonomer NOE restraints from the half-filtered spectrum were flagged to prevent ARIA from rejecting these restraints at early stages of the structure calculation. Although we generate identical distance restraints for each monomer because we observe a single set of resonances, no symmetry restraints are applied in the structure calculations, and the ARIA iterative assignment procedure is free to alter NOE assignments in an asymmetric manner. Beginning with two BNIP3 TMD peptide-extended monomers, ARIA calculated 50 conformers using simulated annealing in CNS, and the 20 lowest-energy structures were selected for further refinement and analysis in a total of nine iterations. Ramachandran statistics were calculated with PROCHECK (*51*), which is embedded in the ARIA suite, and PYMOL (DeLano Scientific) was used to visualize the structures.

RESULTS

Low Mole Fractions of Phospholipids Alter BNIP3 TMD Peptide NMR Spectra in DPC Micelles. Samples of the purified 35-amino acid BNIP3 TMD peptide reconstituted in the detergent dodecylphosphocholine (DPC) give reasonably well dispersed ^{1}H−^{15}N HSQC spectra (Figure 1A), but modifying the pH or altering the reconstitution conditions did not enable us to detect all 33 potentially observable amide peaks. Most amide correlations were similar in intensity; however, several resonances were faint, broad, or observable only in select preparations, and several amides, including those subsequently assigned as Ser 172 and His 173, were present as two peaks, suggesting that the peptide was not conformationally

homogeneous. To test for a possible role of phospholipids in stabilizing the peptide conformation, we added dipalmitoylphosphatidylcholine (DPPC) solubilized in DPC micelles to NMR samples of peptide previously reconstituted in 5% DPC. Adding 2.5 mM DPPC (2.5 lipids per peptide, 1 lipid per 50 detergent molecules) considerably improved the appearances of many peaks in the $^{1}H-^{15}N$ HSQC spectrum (Figure 1B); additional improvements were seen when the lipid concentration was increased to 5 and 7.5 mM (not shown), with little further change seen at 10 mM (Figure 1C). Using the assignments obtained from the sample at 10 mM DPPC, the peaks whose intensities increased upon titration with DPPC correspond to every amide resonance from Lys 163 through His 173. Many of these resonances, including Ser 172, experience systematic changes in ^{1}H and/or ^{15}N chemical shift with lipid titration (Figure 1 of the Supporting Information). It appears that the addition of lipid stabilizes a single conformation of the N-terminal portion of the transmembrane domain and the juxtamembranous region without greatly affecting the C-terminal part of the peptide. We note that the chemical shift heterogeneity observed by Arseniev and colleagues for the amides of Ser 172 and Ala 176 (*42*) is absent in our optimized samples.

Inspection of the methyl regions of $^{1}H-^{13}C$ HSQC spectra of these same samples reveals considerable heterogeneity in the lipid-free samples that is eliminated by DPPC titration. Both the γ and δ methyls of Ile 156 give multiple peaks in the absence of lipid, whereas the methyls of Ile 177, Ile 181, and Ile 183 give single peaks with or without DPPC (Figure 1D–F). In the absence of lipid, the γ methyls of Val 164 also give multiple peaks, which collapse into two peaks at 10 mM DPPC. The leucine δ methyl region is quite crowded, so that the additional peaks seen at low lipid cannot be assigned with certainty from the spectra at 10 mM DPPC; however, it appears that at least one Leu 169 δ methyl is greatly enhanced and that both δ methyls of Leu 162 and Leu 166 are enhanced upon lipid titration. These findings agree with the conclusions drawn from the amide spectra that the N-terminal region of the TMD and the N-terminal juxtamembranous region are most affected by DPPC titration. The observation that the resonances of Ile 156 γ and δ methyls are affected by lipid titration shows that the lipid influence extends nearly to the peptide N-terminus. Although we use $^{1}H-^{15}N$ HSQC (or TROSY) as the primary tool for evaluating conformational homogeneity of membrane peptide samples, 2/J CT $^{1}H-^{13}C$ HSQC identified the existence of multiple conformations more readily in this instance. The presence of multiple peaks in these spectra was not significantly affected by a change in the acquisition temperature, by freezing and thawing, or by maintaining the samples at 80 °C for extended periods prior to the acquisition of data.

The dramatic improvements in BNIP3 TMD peptide spectra upon DPPC titration led us to test other lipids for similar effects. Phosphatidylcholines are abundant in the mitochondrial membranes targeted by BNIP3, but so are phosphatidic acids. Adding detergent-solubilized dipalmitoylphosphatidic acid (DPPA) to BNIP3 peptide in DPC resulted in a similar improvement to N-terminal amides in the $^{1}H-^{15}N$ HSQC spectra (not shown) as seen with the DPPC titration. However, close inspection reveals that the presence of 10 mM DPPA also induces conformational heterogeneity of residues in the C-terminal region of the peptide. The $^{1}H-^{15}N$ HSQC spectra of DPPC- and DPPA-titrated peptide show that many single peaks in the DPPC sample (Figure 2A) appear as double peaks in the DPPA sample

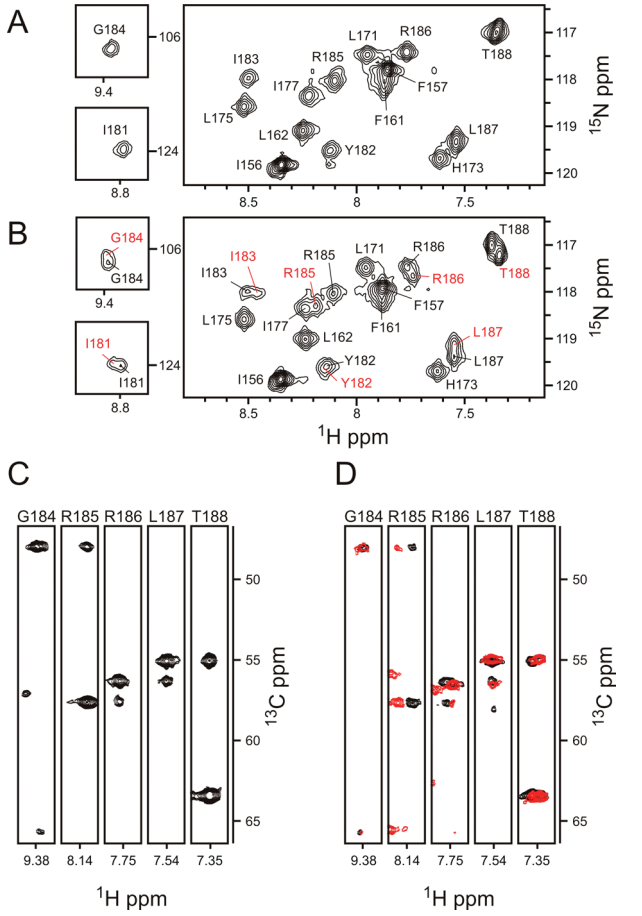

FIGURE 2: Backbone assignments of the C-terminal region of the BNIP3 TMD peptide in the presence of 10 mM DPPC or DPPA. Selected regions of 2D $^{1}H-^{15}N$ HSQC spectra at 800 MHz, 40 °C, 5% DPC, and pH 5.1 in the presence of (A) 10 mM DPPC or (B) 10 mM DPPA are shown with peak assignments. Peaks seen in DPPC as well as in DPPA are labeled in black; peaks seen in DPPA but not DPPC are labeled in red. Strips from the 3D HNCA spectrum of the DPPC sample are shown in panel C in black; each plot is centered at the ^{15}N plane of the indicated backbone amide. For strips from the HNCA spectrum of the DPPA sample (D), plots for each of the two observed amides are presented as overlays. The plot from the ^{15}N plane of the amide peak seen in both DPPC and in DPPA is colored black. The plot from the ^{15}N plane of the amide peak seen only in the DPPA sample is colored red (the corresponding amides are labeled in red in panel B).

(Figure 2B). Additional peaks are clearly associated with amides from the C-terminal region of the TMD (Ile 181, Ile 183, Gly 184, Arg 185, Arg 186, Leu 187, and Thr 188). We assigned the backbone resonances of both the DPPC sample and the DPPA sample using standard through-bond triple-resonance methods. Whereas a single set of resonances is observed for the DPPC sample in HNCA slices (Figure 2C), two conformations with similar intensities but slightly different chemical shifts exist for the amides of residues Ile 181–Thr 188 in the DPPA sample (Figure 2D). The existence of at least two conformations at the C-terminal end of the peptide in DPC and DPPA is further supported by the methyl regions of $^{1}H-^{13}C$ HSQC spectra (see Figure 2 of the Supporting Information).

Resonance Assignments and Structure Determination of the BNIP3 TMD Peptide. Given the varying quality of the spectra under different sample conditions, we chose to pursue side chain assignment and structure determination of the BNIP3 TMD peptide in 5% d_{38}-DPC and 10 mM d_{75}-DPPC at pH 5.1. Using standard triple-resonance methods, we assigned 97% of

Table 1: Observed His 173 Chemical Shifts and Expected Shifts[a] for His Tautomers and the Protonated State

	neutral tautomers		charged	observed
	Nε2H (ppm)	Nδ1H (ppm)	Nε2H/Nδ1H (ppm)	His 173 (ppm)
Cγ	136.8	128.8	129.7	128.0
Cδ2	121.9	128.5	120.2	126.3
Cε1	140.9	141.3	136.5	135.5
Nδ1	249.5	167.5	176.5	167.3
Nε2	167.5	249.5	176.5	

[a] Expected chemical shift values were taken from refs (*52*) and (*53*). It is not clear which nitrogen of His 173 has a shift of 167.3 ppm.

backbone resonances, 95.8% of all peptide hydrogens, and 100% of all nonexchangeable peptide hydrogens. The 2D and 3D correlation spectra reveal only a single set of resonances, consistent with a single symmetric conformation for each monomer within the dimer. Nine exchangeable hydrogens are not observed: the amino terminus, the three serine Hγ atoms, the threonine Hγ atom, the tyrosine Hη atom, the histidine Hδ1 and Hε2 atoms, and the lysine Hζ atom. All observed chemical shifts are well within expected ranges; indeed, the chemical shift dispersion is quite low. As listed in Table 1, the chemical shifts of His 173 do not permit us to assign the side chain as charged or as a given tautomer. The His 173 Cε1 chemical shift is consistent with a protonated side chain (*52*); the Cδ2 shift is more consistent with the Nδ1H neutral tautomer than with the Nε2H tautomer or a charged side chain (*52*), and the Cγ chemical shift is more consistent with the charged state or the Nδ1H tautomer than with the Nε2H tautomer (*52*). No two- or three-bond $^{1}H-^{15}N$ correlations between Hδ2 or Hε1 and the imidazole nitrogens could be detected; the failure to detect two- or three-bond $^{1}H-^{15}N$ correlations has been reported for a histidine in slow to intermediate exchange between a neutral tautomer and the charged side chain (*53*). We obtained a single Hε1/Cε1/N correlation at a ^{15}N chemical shift of 167.3 ppm (Table 1) that could be either Nδ1 or Nε2 and is consistent with the protonated nitrogen of a neutral tautomer. The conflicting chemical shift data mean we cannot assign the tautomeric state of His 173. For the purposes of our calculations and deposited structures, we represent His 173 as having both exchangeable hydrogens because it is easier for most users to remove a hydrogen atom than to add one.

Chemical shift index analysis (*54*) of the Hα, Cα, C′, and Cβ chemical shifts indicates that the peptide is α-helical from Ala 159 to Lys 163 and from Leu 166 to Arg 186, with all other residues scoring as random coil (Figure 3 and Figure 3 of the Supporting Information). Backbone NOE cross-peak patterns also indicate that the peptide is α-helical on these intervals (Figure 3), although in a few instances these NOEs are ambiguous due to chemical shift overlap. On the basis of these data, we applied helical torsion angle restraints (ϕ and ψ) and hydrogen bonding distance restraints for residues 168−185. Using spin−echo difference methods (*45*, *46*), we acquired *J* coupling data that directly yielded 11 χ_1 restraints and other *J* coupling data that when combined with NOE intensity data yielded four χ_2 torsion restraints.

Our initial structure calculations are based on 981 NOEs from 3D (^{15}N- or ^{13}C-separated) NOESY-HSQC spectra and 33 unambiguous intermonomer distance restraints from a half-filtered 3D CN-NOESY-HSQC spectrum (Table 2) (*44*). Because

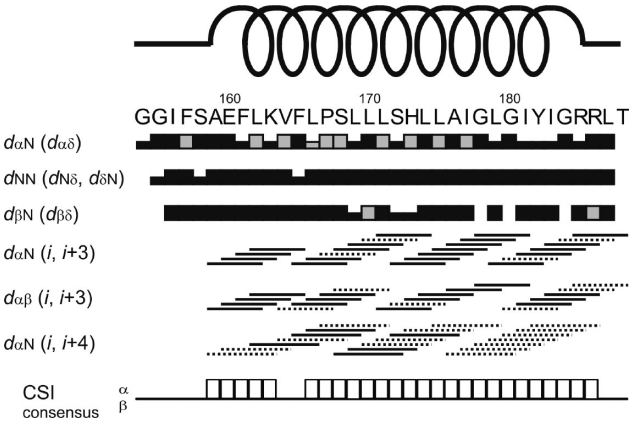

FIGURE 3: Chemical shifts and NOE patterns identify a long α-helix in the BNIP3 TMD peptide. Intraresidue or sequential NOEs consistent with α-helical backbone geometry are indicated by solid blocks (strong peaks), half-blocks (moderate peaks), or gray blocks (strong peaks with redundant chemical shifts). Short-range interresidue NOEs consistent with α-helical backbone geometry are indicated by solid lines or by dotted lines when chemical shift redundancy affects the identification of the peak. Chemical shift index consensus scores are presented as boxes. Overall scores for chemical shift index are presented as white boxes; complete secondary shifts are available in Figure 3 of the Supporting Information.

Table 2: Assignments for Observed Half-Filtered NOE Cross-Peaks and Intermonomer Distance Restraints Calculated from the Peak Volumes by ARIA

		distance (Å)	lower bound (Å)	upper bound (Å)
Leu 169 Hδ1	Phe 165 (Hε or Hζ)	3.5	1.5	1.5
Leu 169 Hδ2	Phe 165 (Hε or Hζ)	3.7	1.7	1.7
Leu 169 Hδ2	His 173 Hε1	3.1	1.2	1.2
Leu 169 Hδ1	Leu 169 (Hδ1 or Hδ2)	3.1	1.2	1.2
His 173 Hα	His 173 Hδ2	3.3	1.3	1.3
Ala 176 Hβ	Ile 177 Hδ1	3.6	1.6	1.6
Ala 176 Hβ	His 173 Hα	3.0	1.2	1.2
Ala 176 Hβ	His 173 Hδ2	2.6	0.8	0.8
Ala 176 Hβ	Ala 176 Hβ	2.5	0.8	0.8
Ala 176 Hβ	Ile 177 HN	3.4	1.5	1.5
Ala 176 Hβ	Ile 177 Hα	3.6	1.7	1.7
Ala 176 Hβ	Ile 177 Hγ12	2.9	1.0	1.0
Ala 176 Hβ	Ile 177 Hγ13	2.7	0.9	0.9
Ile 177 Hδ1	Ala 176 Hα	3.5	1.5	1.5
Ile 177 Hδ1	Leu 179 Hδ1	2.6	0.9	0.9
Ile 177 Hγ2	Leu 179 Hβ2	3.8	1.8	1.8
Ile 177 Hγ2	Gly 180 Hα2	3.5	1.5	1.5
Ile 177 Hγ2	Ile 177 Hα	4.3	2.3	1.7
Ile 177 Hγ2	Leu 179 Hβ3[a]	3.8	1.8	1.8
Ile 177 Hγ2	Gly 180 HN	3.2	1.3	1.3
Ile 177 Hγ2	Gly 180 Hα3	3.2	1.3	1.3
Ile 177 Hα	Ile 177 Hα	3.3	1.3	1.3
Leu 179 Hγ	Ile 177 Hγ2	4.2	2.2	1.8
Gly 180 HN	Ile 177 Hα	3.3	1.3	1.3
Ile 181 Hγ2	Gly 184 Hα2	3.4	1.5	1.5
Ile 181 Hγ2	Gly 184 Hα3	3.4	1.5	1.5
Ile 181 Hγ2	Gly 184 HN	4.1	2.1	1.9
Ile 181 Hγ2	Ile 183 Hδ1[a]	2.9	1.1	1.1
Ile 181 Hα	Ile 183 Hγ2[a]	4.4	2.5	1.6
Ile 181 Hα	Gly 184 Hα2	3.3	1.3	1.3
Ile 181 Hα	Gly 184 Hα3	4.4	2.5	1.6
Ile 183 Hβ	Ile 181 Hδ1	3.5	1.5	1.5
Gly 184 HN	Ile 181 HA	3.2	1.3	1.3

[a] Assignments for which ambiguities remain because of chemical shift redundancies, even after iterative ARIA calculations.

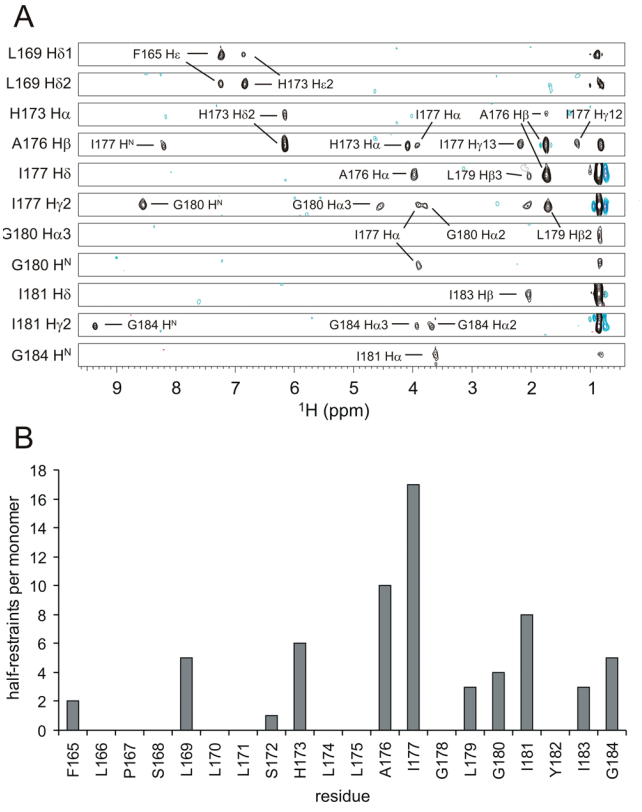

FIGURE 4: Unambiguous intermonomer NOEs and distance restraints. (A) Strips from a 3D half-filtered NOESY spectrum acquired on a mixture of labeled and unlabeled BNIP3 TMD peptide are shown for hydrogens of residues that participate in at least three intermonomer NOEs. Peaks assigned on the basis of chemical shift alone are labeled; some unlabeled peaks were assigned by ARIA. Redundancy in methyl ^{1}H chemical shifts (14 methyls between 0.80 and 0.88 ppm) complicates assignment of peaks at these indirect ^{1}H shifts, but the same structural information is obtained from strips where the methyls are resolved from one another in the ^{13}C and direct ^{1}H dimensions and the NOE partner is identified by a more unique indirect ^{1}H shift. For instance, the upfield peak in the G180 H^N strip cannot be unambiguously assigned on the basis of the indirect ^{1}H chemical shift, but the strip for I177 Hγ2 shows a peak at the shift of G180 H^N. (B) Distribution of intermonomer distance restraints along the peptide sequence. Each unique NOE peak has been counted twice: once for the residue of the directly observed hydrogen and once for the residue of the hydrogen in the indirect dimension. Redundant peaks that give the same information from different parts of the 3D spectrum have been eliminated from this count. For instance, the close intermonomer approach of G180 H^N and I177 Hγ2 results in a cross-peak in both the G180 H^N column and the I177 Hγ2 column of the half-filtered NOESY spectrum. One of these peaks is discarded, and the remaining peak counts for both G180 and I177.

the sample contains a mixture of unlabeled and fully ^{15}N- and ^{13}C-labeled BNIP3 TMD peptide, NOE cross-peaks in the half-filtered spectrum can arise only from cross-relaxation of hydrogens on one monomer by hydrogens on the other monomer. Ten residues exhibit intermonomer NOEs, and seven residues participate in more than three such NOEs: Leu 169, His 173, Ala 176, Ile 177, Gly 180, Ile 181, and Gly 184. Strips from the half-filtered NOESY-HSQC spectrum for hydrogens from each of these residues are presented in Figure 4A, and the distribution of NOE-derived intermonomer distance restraints along the sequence is depicted in Figure 4B. Many NOE peaks are observed at the direct ^{1}H chemical shift of each NOE partner, resulting in redundant NOE information; Figure 4 reports the number of independent intermonomer distance restraints after doubly counted peaks had been filtered out. Most NOE peaks were assigned by hand, but some assignments were obtained during iterative cycles of assignment and structure calculation with ARIA 1.2 (*49*) (see Experimental Procedures). With ~30 NOEs per residue and 33 unambiguous intermonomer NOEs, we have sufficient restraints to define the structure with good precision.

Structure of the BNIP3 TMD Dimer. Structure determination using ARIA 1.2 (see Experimental Procedures) yielded an ensemble of 20 low-energy structures (Protein Data Bank entry 2ka1, BMRB accession number 16012) that satisfy the restraints of the NMR data (Table 3). Figure 5 shows the family of BNIP3 TMD peptide dimer structures and a stereopair close-up of the interacting region. The structures indicate that the BNIP3 TMD peptide dimer is symmetric and crosses with a right-handed orientation, with a crossing angle of approximately −34°, and there is a high degree of convergence of the family of structures, particularly in the membrane-spanning region (residues 167−184). The dimer interface is composed of residues 172, 173, 176, 177, 180, 181, and 184. We previously identified five of these residues as being important for BNIP3 TMD dimerization on the basis of mutagenesis data (*30*). The dimer is closely packed, especially at positions 176−184, with the closest approach of the helices near Gly 180, where the Cα−Cα distance between the two monomers is 4.0 ± 0.3 Å.

Intermonomer Side Chain Hydrogen Bonds at the BNIP3 Dimer Interface. Although the exchangeable hydrogens of His 173 are not observed, structure calculations that include half-filtered NOEs to the nonexchangeable Cδ2H and Cε1H protons consistently orient the His side chain close to a favored rotamer (*3*) for α-helices ($\chi_1 = -74°$; $\chi_2 = 82°$) and in position to participate in an intermonomer hydrogen bond between His Nε2 and the Oγ atom of Ser 172 (see Table 4). For the sake of symmetry in our structure calculations, His 173 is always present as the protonated imidazole; removal of Nδ1H (or Nε2H) from one or both monomers in the dimer could also be consistent with the chemical shift data (assuming rapid exchange). If Nε2H is removed, the hydroxyl proton of Ser 172 on the opposite monomer can rotate to enable this side chain to donate, rather than accept, the hydrogen bond. The structure of the BNIP3 TMD dimer therefore indicates that His−Ser intermonomer hydrogen bonds form across the BNIP3 helix−helix dimer interface, supporting our previous conclusion that BNIP3 dimerization is stabilized by intermonomer hydrogen bonds between His 173 and Ser 172 (*30*).

The electronegative atoms inferred to form intermonomer hydrogen bonds in the family of structures described above are farther apart than what we would expect for a canonical interaction. We expect that this geometry results in part from our lack of experimental distance restraints for the exchangeable hydrogens of the His 173 imidazole ring and the Ser 172 hydroxyl; all three of these hydrogens exchange rapidly with the solvent. To test whether the available experimental data are consistent with an idealized intermonomer hydrogen bond, we added a pair of intermonomer His Nε2−Ser Oγ hydrogen bond distance restraints and recalculated the structures. The new family of structures (Protein Data Bank entry 2ka2) satisfies the experimental restraints equivalently well (see Table 3) and positions the His 173 side chain to form a shorter, more ideal hydrogen bond between His 173 Nε2 and Ser 172 Oγ (see Table 4). Interestingly, adding these hydrogen bond restraints brings the side chain dihedrals for His 173 closer to a rotameric state. This rotamer positions the imidazole ring so that His 173 Nδ1H, if present, could make a favorable intramonomer hydrogen bond with the

Table 3: NMR Structural Statistics[a] and Atomic Root-Mean-Square Differences

	2ka1	2ka2
Experimental Restraints per Monomer		
no. of NOE restraints		
intraresidue	622	622
inter-residue		
sequential	192	192
medium-range	114	114
long-range	53	53
unambiguous intermonomer	33	33
no. of hydrogen bond restraints	29	29
no. of torsion angle restraints		
backbone ϕ	17	17
backbone ψ	17	17
side chain χ_1	11	11
side chain χ_2	4	4
no. of inferred intermonomer hydrogen bonds	0	1
Structure Statistics		
restraint violations		
distance (>0.5 Å)	0	0
distance (>0.3 Å)	0.05	0
dihedral (>5°)	0	0
deviation from idealized geometry		
bonds (Å)	0.0011 ± 0.0001	0.0012 ± 0.0001
angles (deg)	0.314 ± 0.006	0.316 ± 0.007
impropers (deg)	0.151 ± 0.010	0.151 ± 0.010
deviation from experimental restraints		
NOE	0.0073 ± 0.0018	0.0083 ± 0.0011
dihedrals (deg)	0.21 ± 0.05	0.26 ± 0.07
rmsd (residues 168−185)		
backbone atoms	0.29 ± 0.08	0.29 ± 0.08
all heavy atoms	0.46 ± 0.11	0.47 ± 0.09
Ramachandran analysis (residues 168−185)		
% residues in most favored region	99.7	99.8
% residues in allowed region	0.3	0.2
% residues in generously allowed region	0.0	0.0
% residues in disallowed region	0.0	0.0

[a] Statistics are calculated and averaged over the 20 lowest-energy dimer structures out of a total of 50 calculated structures.

carbonyl oxygen of Leu 169 (the $i-4$ residue of the same helix). The crossing angles from the two families of structures do not differ significantly ($-34.1 \pm 2.6°$ compared to $-32.9 \pm 2.3°$ when the intermonomer hydrogen bond is added), and the rmsd of the backbone atoms of one family onto the average structure of the other family is only 0.51 Å, indicating that the inclusion of the inferred intermonomer hydrogen bond does not significantly alter the global conformation of the BNIP3 dimer structure. We conclude that the NMR data defining the BNIP3 dimer interface are consistent with formation of a short intermonomer hydrogen bond between His 173 Nε2 and Ser 172 Oγ.

The only atoms from residues 165−187 that show NOEs to water are His 173 NH, Cδ2H, and Cε1H. These correlations to imidazole hydrogens presumably arise from cross relaxation with Nδ1H and Nε2H, which are in rapid exchange with solvent and are not observed in $^{15}N-^{1}H$ correlation experiments. At pH 5.1, rapid exchange of the His 173 amide proton itself is not feasible, but the histidine rotamer described above places Nδ1H in the proximity of the His 173 backbone amide proton (~2.4 Å). Thus, rapid exchange of Nδ1H and Nε2H with solvent would explain all NOE cross-peaks seen to the water frequency for the hydrophobic membrane-spanning region of the BNIP3 peptide. The absence of any other cross-peaks to the solvent indicates that water does not partition significantly into this region of the mixed micelle.

Noncanonical Intermonomer Hydrogen Bonds or Polar Interactions. The close approach of two BNIP3 helices in our structure permits intermonomer backbone−backbone packing interactions that include slightly polar interactions or noncanonical hydrogen bonding. Helix−helix packing afforded by GxxxG TMD dimerization motifs may permit Cα−H·O=C noncanonical hydrogen bonds to form, and the energetic contributions of these interactions could be significant in apolar environments (*55*). Analysis of our family of structures reveals four such potential contacts (Table 5 and Figure 6), each of which occurs twice in the symmetric homodimer. The geometric parameters listed in Table 5 do not change significantly for structures calculated with (Protein Data Bank entry 2ka2) or without (Protein Data Bank entry 2ka1) the inferred intermonomer hydrogen bonds. On the basis of geometric criteria, three of these interactions are likely to constitute hydrogen bonds, whereas the G184−I181 interatomic separations are too large. Because interatomic distances in NMR structures are strongly dependent on the energy function used to represent van der Waals interactions in the structure calculation, we looked for evidence of noncanonical hydrogen bonding in our primary NMR data. Quantum mechanical calculations indicate that α hydrogens involved in hydrogen bonds to carbonyl oxygens would experience significant (1.5 ppm) perturbations in chemical shift (*56*). The Gly 180 Hα2 shift is 0.75 ppm downfield from Hα3 and 0.91 ppm downfield from the average Hα2/Hα3 shifts of Gly 178, which, like Gly 180, is in a helix. [Gly 180 Hα2 is sufficiently downfield that it scores as "sheet" in chemical shift index analysis (see Figure 3 of the Supporting Information.)] This chemical shift outlier indicates a unique environment for Gly 180 Hα2 that is consistent with deshielding caused by noncanonical hydrogen bonding. Because the Hα resonances of other candidate hydrogen bond donors in Table 4 do not show strong chemical shift perturbations, we are reluctant to classify these as noncanonical hydrogen bonds. Even if true hydrogen bonds are not formed, polar interactions between these atoms could still contribute significantly to dimer stability and specificity, as previously shown by a purely electrostatic calculation of the contribution of Cα−H·O=C interactions to transmembrane helix−helix energetics (*57*). We conclude that the structure contains a pair of noncanonical intermonomer hydrogen bonds between Gly 180 and Ile 177, as well as two more pairs of backbone−backbone polar contacts that could stabilize or contribute to the specificity of BNIP3 helix−helix interactions.

Structural Rationalization of the Effects of Mutations on Dimerization. We previously determined how 200 point mutations affect BNIP3 TMD dimerization in detergent and drew inferences about the nature of the dimer interface (*30*). In that study, the effects of hydrophobic substitutions provided the most distinct periodic disruption pattern, which we interpreted as defining an interacting surface (*30*). A comparison of this disruption pattern with the packing of the dimer structure interface is shown in Figure 7A, which indicates how many intermonomer contacts of ≤4.5 Å are made by non-hydrogen atoms of each residue in the average structure. Although many positions that show packing contacts in the structure are

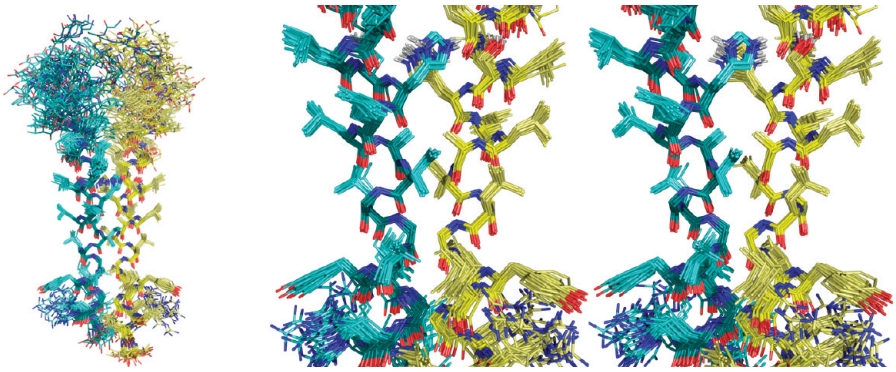

FIGURE 5: Family of BNIP3 TMD NMR structures. (A) All heavy atoms of the family of 20 NMR structures (Protein Data Bank entry 2ka1) are shown, superimposed using the backbone atoms of residues 168−185 with the N-terminal end at the top. Main chain atoms of individual monomers are colored deep teal or yellow, and side chain atoms are shown in a lighter shade. (B) The well-defined backbone and side chain atoms of the interacting region are shown as a wall-eyed stereopair; the polar hydrogens of Ser 172 and His 173 side chains are shown to illustrate the nature of the intermonomer hydrogen bonds.

Table 4: Geometry of His 173 and Ser 172 in Families of Structures Calculated Using NMR Data Alone (2ka1) or Including an Inferred Intermonomer Hydrogen Bond Distance Restraint (2ka2)

	His 173 χ_1 (deg)	His 173 χ_2 (deg)	Nε−Oγ distance (Å)	Nε−NεH−Oγ angle (deg)
2ka1	−65 ± 3	115 ± 10	4.19 ± 0.30	143 ± 12
2ka2	−63 ± 2	99 ± 6	3.09 ± 0.11	150 ± 7

Table 5: Intermonomer Contacts That May Constitute Noncanonical Hydrogen Bonds[a]

C^α−H^α	O=C	ζ (deg)	ξ (deg)	θ (deg)	d_H (Å)	d (Å)
	ideal	180	120	0	< 2.7	< 3.8
	range	90−180	100−170		< 3.5 if ξ = 120°	
			2ka1			
Ile 177	Ala 176	149 ± 6	110 ± 6	−65 ± 15	2.7 ± 0.2	3.6 ± 0.2
Gly 180	Ile 177	144 ± 8	133 ± 9	86 ± 15	2.6 ± 0.2	3.5 ± 0.2
Ile 181	Gly 180	133 ± 9	109 ± 7	−35 ± 15	2.6 ± 0.3	3.4 ± 0.3
Gly 184	Ile 181	147 ± 10	114 ± 9	93 ± 21	3.7 ± 0.4	4.6 ± 0.4
			2ka2			
Ile 177	Ala 176	146 ± 7	112 ± 7	−60 ± 13	2.5 ± 0.2	3.4 ± 0.2
Gly 180	Ile 177	142 ± 8	131 ± 11	89 ± 14	2.6 ± 0.2	3.5 ± 0.2
Ile 181	Gly 180	134 ± 10	113 ± 9	−18 ± 18	2.6 ± 0.3	3.4 ± 0.3
Gly 184	Ile 181	143 ± 9	114 ± 10	100 ± 18	3.4 ± 0.3	4.3 ± 0.3

[a] Nomenclature and ranges are from refs (*55*) and (*69*): ζ is the C^α−H^α−O angle, ξ is the H^α−O=C angle, θ is the C^α−H^α−O=C torsion angle, d_H is the H^α−O distance, and d is the C^α−O distance.

associated with a highly disruptive phenotype, the rank order of importance for the mutagenesis data and structural parameters are not in agreement. Ile 181 and Ile 177 rank fourth and fifth in intermonomer contacts, respectively, ahead of Gly 184, but only eighth and eleventh, respectively, in the mutagenesis disruption scale; indeed, dimerization is unaffected by hydrophobic substitutions at Ile 177. Conversely, Ser 172 ranks seventh on the packing scale but is tied with three other positions at the top of the mutagenesis scale: every substitution at Ser 172 fully disrupts dimerization. These rankings demonstrate that although the positionally averaged effect of hydrophobic substitutions on dimerization correctly identifies most interfacial residues, the mutational data cannot be directly translated into a scale for van der Waals contacts.

To seek structural explanations for the effects of hydrophobic substitutions at the BNIP3 TMD dimer interface, we used molecular modeling to assess how these mutations would affect the interface. We built each mutant side chain into the average NMR structure using PYMOL (DeLano Scientific), considering each possible backbone-dependent rotamer (*3*, *58*) for the mutant residue to determine if, without altering the backbone geometry, the mutation would cause a clash. Mutations for which every rotamer causes a clash are indicated with an asterisk in Figure 7B; for mutations that can be accommodated sterically in at least one rotamer, we indicate if the replacement would significantly increase (+) or decrease (−) the number of intermonomer packing contacts or if the His 173−Ser 172 intermonomer hydrogen bond would be eliminated (h). Mutations for which the side chains point away from the dimer interface cause no change (nc) in intermonomer contacts.

Our mutational analysis identified the AxxxGxxxG motif as being critical to dimerization (*30*), and the effects of substitutions at these positions (see Figure 7B) are readily explained by building the substitutions into the wild-type NMR structure

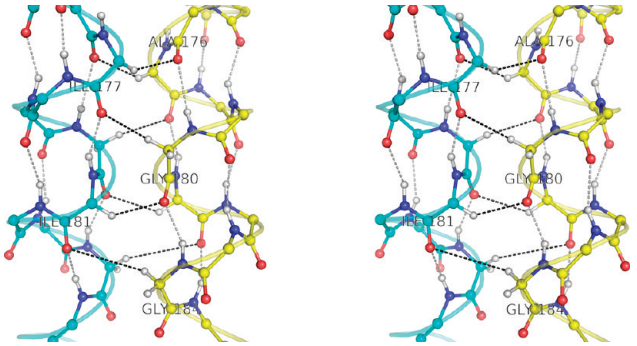

FIGURE 6: Stereo pair of backbone contacts at the BNIP3 dimer interface. Backbone atoms including amide hydrogens are shown in a ball-and-stick representation for both helices. α hydrogens possibly involved in noncanonical hydrogen bonds are also shown, and the intermonomer Cα−H·O═C polar contacts are represented with dark dotted lines in the front half of the dimer and medium dotted lines in the back half. Intramonomer helical hydrogen bonds are represented by light dotted lines.

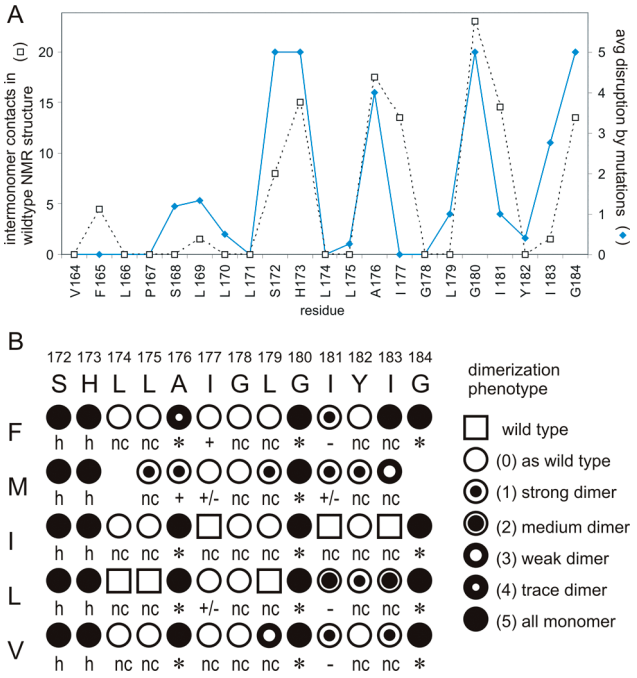

FIGURE 7: Comparison of mutagenesis data and the NMR structure. (A) The number of intermonomer contacts per residue (≤4.5 Å between non-hydrogen atoms) for the averaged and energy-minimized structure is indicated by the white squares (dotted lines), with the scale at the left. The average disruptive effect of hydrophobic substitutions from ref (*30*) is indicated by the blue diamonds (solid line); on the scale at the right, 5 indicates complete disruption and 0 indicates dimerization as the wild type. (B) The effects of hydrophobic substitutions on BNIP3 TMD dimerization in detergent (*30*) are indicated with a numeric scale (0−5) and a symbol in which increasing number or amount of black corresponds to an increasing level of disruption. The effects on intermonomer contacts of each substitution in the wild-type structure using ideal rotamers (see Experimental Procedures) is scored nc if there are no changes, * if a clash is introduced, + if the number of packing contacts increases, − if the number of packing contacts decreases, ± if several rotamers are possible with a range of packing effects, and h if the His−Ser intermonomer hydrogen bond is lost. The most disruptive phenotypes correlate with intermonomer contact scores of * and h.

(Figure 8). The close packing between the two monomers (Figure 8A) can sterically accommodate replacement of Ala 176 with a cysteine in a favorable rotamer (Figure 8B), but placing a valine at this position causes a clash with the backbone and side chain atoms of Ile 177 of the opposite monomer (Figure 8C). At Gly 180, where the helix backbones are in van der Waals contact, even an alanine substitution causes clashes with the carbonyl oxygen of Ile 177 and backbone and side chain atoms of Ile 181 (Figure 8D). We attribute the almost universally disruptive effects of small-to-large mutations at the AxxxGxxxG motif positions to steric clashes.

If the glycine zipper motif is excluded, the residues that make the most intermonomer van der Waals interactions are Ile 181 and Ile 177. Ile 181 packs against Gly 180 and also contacts Gly 184 and Ile 183; Ile 177 packs primarily against Ala 176 but also contacts Gly 180. Despite this extensive packing, the mutagenesis data show that hydrophobic substitutions at Ile 181 only moderately decrease the level of dimerization, and Ile 177 accepts any hydrophobic residue without affecting dimerization at all (*30*). Building the mutations into the wild-type structure shows that none of the substitutions results in a clash; rather, the hydrophobic substitutions can always be accommodated in a favorable rotamer. At position 181, such rotamers usually point away from the dimer interface and thus make fewer favorable intermonomer contacts than the wild-type residue, but half the intermonomer contacts made by Ile 181 involve the N, Cα, or Cβ atom and are thus unaltered by these mutations. The number of contacts lost is less than 5% of the total number of contacts in the wild-type structure; this apparently has only a moderate effect on dimer stability. At position 177, some substitutions can be accommodated in rotamers that match or exceed the number of favorable packing contacts seen in the wild-type structure, explaining the lack of disruption observed for these mutations.

Residues 172 and 173 make only a moderate number of steric contacts with the opposite monomer; these contacts occur entirely between side chain atoms because the crossing angle of the helices results in a large separation between the backbones at these positions. Despite the small numbers of contacts between the monomers, hydrophobic mutations at these two residues completely disrupt dimerization. These substitutions do not result in clashes: more than one compatible rotamer combination can always be identified, though bulky side chains often must point away from the opposite monomer and therefore make few favorable intermonomer contacts. However, the number of steric contacts lost is smaller than for changes at Ile 181, where mutations have a minimal effect on dimerization. In all cases, however, hydrophobic substitutions would abolish the side chain−side chain hydrogen bonds between His 173 and Ser 172. We therefore attribute the strongly disruptive effects of hydrophobic substitutions at Ser 172 and His 173 primarily to the loss of hydrogen bonding interactions between side chains.

One additional position, Ile 183, was implicated in our mutational analysis as contributing to intermonomer interactions (*30*). Ile 183 is near the interface and participates in two intermonomer NOEs, but it does not make significant packing interactions across the dimer interface. Hydrophobic substitutions at this position neither generate clashes nor result in any significant loss of packing interactions. Accordingly, we conclude that the range of disruptive effects of hydrophobic substitutions at Ile 183 cannot be explained by a simple steric model based on the wild-type dimer NMR structure. This contrasts sharply with hydrophobic substitutions at all other positions analyzed for this system, where clashes, loss of favorable packing interactions, and loss of hydrogen bonding interactions successfully rationalize the effects of mutations.

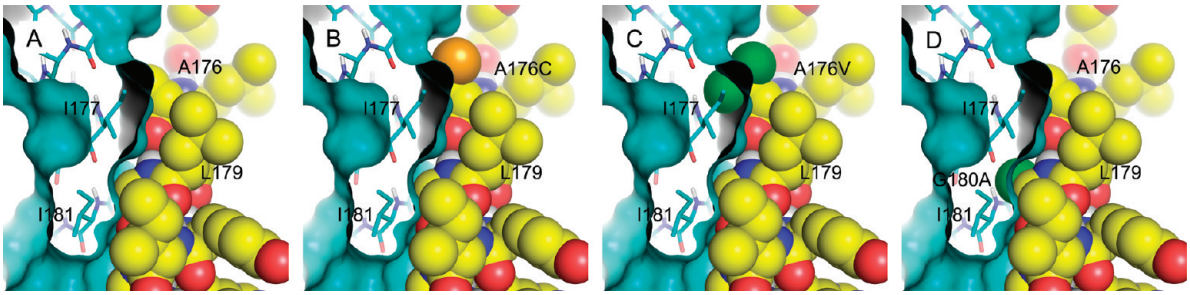

FIGURE 8: Modeling mutations at the BNIP3 TMD dimer interface. The average NMR structure (A) is presented with one monomer as van der Waals spheres and the other monomer as a molecular surface over a stick model. Hydrogens are omitted except for amide hydrogens, and the molecular surface is cut away to facilitate visualization of packing and steric clashes. Identical views show that the Ala176Cys substitution is accommodated without steric clash (B): one available favorable rotamer places the Sγ atom (gold) near the interface without penetrating the molecular surface of the opposite monomer. In contrast, the only available rotamer for the Ala176Val substitution (C) forces one of the two γ methyls (green) to clash with the opposite monomer. The single methyl added for the Gly180Ala mutation (D) also causes a severe clash with the opposite monomer.

DISCUSSION

The Structure of the BNIP3 TMD Peptide Dimer Supports the Central Arguments Based on Saturation Mutagenesis. The structure of the BNIP3 TMD peptide dimer indicates that the helices interact with a right-handed crossing angle of approximately −34°, with Gly 180 at the crossing point and small residues Ala 176, Gly 180, and Gly 184 buried at the dimer interface. All three of these residues were identified on the basis of mutagenesis data as being critical to dimerization (*30*), and the structure confirms the role of both glycines in permitting backbone−backbone contacts between monomers. Small-to-large substitutions at all three positions disrupt the dimer because they cause clashes with the other monomer. The structure shows that the His 173 side chain Nε2 atom of each monomer participates in a hydrogen bond with the side chain γ oxygen of Ser 172 on the opposite monomer. These two residues were also identified by mutagenesis as being critical to dimerization, and we conclude that the disruption associated with hydrophobic substitutions at these positions is caused by loss of the intermonomer hydrogen bonds. The five residues identified by mutagenesis as being most critical to dimerization (Ser 172, His 173, Ala 176, Gly 180, and Gly 184) (*30*) are therefore confirmed by the structure to play critical roles in determining intermonomer contacts that contribute to dimer stability.

Mutagenesis Did Not Correctly Identify All Residues That Participate in the Dimer Interface. Inferences based on mutagenesis results for other positions, however, are not as well supported by the structure. Mutational analysis implicated Ile 183 in dimerization, and although the structure places this residue at the interface, the mutations that disrupt dimerization would not be expected to cause steric clashes or eliminate favorable van der Waals contacts. As such, the residue thought to make the sixth-most important contributions to dimerization based on mutagenesis (*30*) has no significant intermonomer contacts in the NMR structure. Further investigation will be needed to determine why these mutations alter dimerization in detergent, and if they affect dimerization in membranes. Since protein−protein contacts do not seem to explain the effects of mutations at position 183, it is possible that interaction of the peptide with detergents or lipids could be affected. Changing the interaction of the BNIP3 TMD with lipids could affect helix formation, which could influence the amount of dimer seen in our assays by decreasing the fraction of correctly folded monomer.

Our previous mutational analysis also failed to identify strong roles for Ile 177 and Ile 181 in dimerization. The lack of disruption by hydrophobic substitutions at these positions is consistent with the wild-type structure because these mutations cause no clashes and do not significantly decrease the number of van der Waals contacts between monomers. We note that alanine or glycine substitutions are strongly or completely disruptive at these two positions (*30*). Such substitutions are also weakly to moderately disruptive at noninterfacial positions, probably because they lower the hydrophobicity of the transmembrane domain and thereby favor unfolding of the helical monomer (*30*). The dramatic effects of alanine or glycine substitutions at positions 177 and 181 may therefore arise from a combination of a decrease in hydrophobicity and a loss of favorable intermonomer van der Waals contacts.

Importance of Hydrogen Bonding to BNIP3 TMD Dimerization. The NMR structure shows that the His 173 Nε2 atom of each BNIP3 monomer forms a hydrogen bond to the side chain oxygen of Ser 172 of the other monomer. In our mutational analysis of BNIP3 dimerization (*30*), every hydrophobic substitution at positions 172 and 173 completely abolished dimerization on SDS−PAGE. Modeling side chains as rotamers shows that the profound effects of these mutations cannot be explained by steric clashes, and that only a few steric contacts are lost with these mutations. We conclude that the large effects of single point mutations at positions 172 and 173 are due primarily to the elimination of two intermonomer hydrogen bonds. However, understanding the energetic contribution of these hydrogen bonds to dimerization will require quantitative thermodynamic studies that can place these His−Ser interactions on a common scale with Gln stabilizing interactions in designed TMDs (*38*) and side chain hydrogen bonding in bacteriorhodopsin (*40*).

Lipids Modulate the BNIP3 TMD Peptide Conformation. The preparation of folded, conformationally homogeneous samples of membrane proteins is still a major bottleneck to studies of membrane protein structure and function. Simply redissolving our dried, HPLC-purified BNIP3 peptide in a detergent solution yields samples that are strongly aggregated and exhibit chemical shift heterogeneity. Even samples reconstituted by codissolving detergent and peptide in a mixture of organic solvent and water, lyophilizing the frozen sample, and redissolving in water, which give reasonable amide spectra (Figure 1A), can show evidence of multiple conformations in the methyl region (Figure 1 D,G). Adding detergent-solubilized

DPPC to our peptide/DPC sample eliminated the chemical shift heterogeneity associated with minor conformations. The DPPC effect is strongest with the first titration aliquot, but the NMR spectra continue to improve in going from 2.5 lipids per peptide to 5, 7.5, and 10 lipids per peptide, suggesting that a tight lipid−peptide complex is not formed. Using protonated lipid, deuterated detergent, and a half-filtered NOESY spectrum, we searched for lipid−peptide contacts but did not identify any significant peaks at 60 ms mixing times (not shown), which supports the idea that there are no tightly bound lipids. At present, we cannot determine whether DPPC influences the spectra by altering the properties of the mixed micelles or by direct interactions with the BNIP3 TMD peptide, but we favor the former explanation.

The ability of DPPC to stabilize a single conformation of the detergent-solubilized BNIP3 peptide dimer is not surprising, since native lipids have been shown to interact with and stabilize membrane proteins (*59*−*61*). The behavior of our samples upon addition of DPPA is more complicated and more difficult to understand. DPPA eliminates chemical shift heterogeneity in the N-terminal part of the membrane span with a concentration dependence similar to that of DPPC but induces chemical shift heterogeneity in the C-terminal part of the peptide, including residues intimately involved in dimerization [Ile 181 and Gly 184 (see Figure 2)]. One possible explanation for these lipid effects is that both DPPA and DPPC alter the properties of the DPC micelle in a way that favors a single peptide conformation in the vicinity of Ser 172 and His 173, whereas negatively charged DPPA (but not zwitterionic DPPC) makes specific interactions with the C-terminal region of the peptide, perhaps through contacts with Arg 185 or Arg 186. Although we chose to pursue structure determination of the fully symmetric peptide dimer in the presence of DPPC, we cannot rule out the possibility that the conformational heterogeneity seen in the C-terminal portion of the peptide in the presence of DPPA could have functional significance, since both PC and PA lipids are present in BNIP3 target membranes.

Lipids are known to interact with membrane proteins over a range of affinities and time scales (reviewed in ref (*62*)). Our finding that addition of lipids to a detergent-reconstituted, strongly delipidated peptide can eliminate (or induce) the formation of alternate peptide conformations indicates that at least some lipid effects are reversible. We suggest that in addition to purifying membrane proteins under conditions that allow them to retain native lipids, select lipids could be reintroduced to purified membrane proteins to optimize the behavior of biophysical and biochemical samples. Given that one native lipid drives the BNIP3 peptide toward a single conformation whereas another promotes heterogeneity, our findings support a strategy of broadly surveying not only detergents (*63*) but also lipid additives when seeking to identify conditions for studying solubilized membrane protein samples. We note that N-terminal conformational heterogeneity persists in BNIP3 peptide samples prepared in bicelles or mixed micelles composed entirely of PC headgroups and containing a significant mole fraction of DMPC (*42*).

Contrast with Previous Structural Conclusions. Within the membrane-spanning segment, our structure resembles a previously reported BNIP3 TMD dimer NMR structure (*42*) and a computational model (*41*). The backbone atoms of residues 172−184 from either the previous family of NMR structures or the computational model superimpose on our average structure at a rmsd of ~0.7 Å, although the helices cross at a wider angle for the previous NMR family (−39.5 ± 4.9°) or for the computational prediction (−41.5°) than for our family (−34.1 ± 2.6°). Despite the similarities of the backbone arrangements, the details of the side chain positions, especially for His 173 and Ser 172, differ substantially among the three methods. Given that the chemical shifts of the backbone and side chain resonances reported here are very similar to those previously reported by Arseniev and colleagues (*42*), it seems likely that differences between the two NMR structures arise mostly from differences in the experimental restraints. The previous family of NMR structures is based on 304 intramonomer and 14 intermonomer NOEs (608 and 28 restraints, respectively) (*42*), whereas the structures presented here are based on 981 NOEs of either intra- or intermonomer origin and 33 strictly intermonomer NOEs (1962 and 66 restraints). The higher number of restraints explains the increased precision of the family of structures described here.

The experimental intermonomer restraints of Arseniev and colleagues [Protein Data Bank entry 2j5d (*42*)] are highly clustered: 9 of the 14 NOEs involve only residues 176 and 177, 2 NOEs involve residues 173 and 176, and 3 NOEs do not involve residue 176 or 177 at all. The 33 intermonomer NOEs listed in Table 2 similarly include 9 NOEs involving only residues 176 and 177, but also 10 NOEs that involve one of these residues and another interfacial residue, and 14 NOEs that do not involve residue 176 or 177 at all. The broad distribution of many intermonomer restraints along the sequence reported here (Figure 4B) is the probable source of the differences in the helix−helix crossing angle of the two studies.

The conformational homogeneity of our samples may explain why we detect more NOEs (and more intermonomer NOEs) than the previous NMR study, and thus why the interaction between His 173 and Ser 172 is more precisely defined in our structures. Differences in observed intermonomer NOEs could also reflect real conformational differences caused by the choices of peptide sequence or lipidic solvent in the two types of sample: our peptide is 35 residues starting at Gly 154, whereas the previous study used a 45-residue peptide starting at Arg 146; our sample is reconstituted in 12.5:1 DPC/DPPC micelles, whereas the previous study used 4:1 DHPC/DMPC micelles. Given the substantial differences in the intermonomer NOEs used to calculate the structures, the similarities between the two sets of structures are more remarkable than the differences.

Both the primary NMR data and the calculated structures lead us to conclusions that differ from those of the previous NMR and MD study. Arseniev and colleagues observed minor peaks (~10%) in addition to major peaks for some resonances in their samples (*42*), and the existence of multiple peaks for Ser 172 and Ala 176 amides led these authors to conclude that slow exchange between alternative BNIP3 dimer interfaces was occurring in their samples. This chemical shift heterogeneity was also offered as experimental support for the existence of long-lived alternate conformations of His 173 and Ser 172 seen in MD simulations (*42*). Our samples exhibit single peaks for all backbone and side chain resonances, demonstrating that the BNIP3 peptide can form a completely symmetric dimer and challenging the idea that distinct backbone or side chain conformations exist in slow exchange. The conformations of His 173 and Ser 172 are well-defined across the family of structures, and His 173 adopts a single favorable rotamer in all cases; on the other hand, the family of structures deposited by Arseniev and colleagues includes alternate His 173 conformations (*42*). Because we can eliminate chemical shift heterogeneity similar to that described by Arseniev

and colleagues by modifying the sample composition and reconstitution protocol, we believe that the BNIP3 TMD dimer, or at least our 35-residue peptide, exists as a single time-averaged conformer from Phe 165 to Gly 184 in which residues His 173 and Ser 172 are positioned to form intermonomer hydrogen bonds. We suggest that these calculated structures provide a more accurate view of the time-averaged conformation of the BNIP3 dimer interface than the Arseniev family, especially for Ser 172 and His 173. Although our data indicate that the BNIP3 dimer does not undergo slow exchange between distinct interfaces, we note that neither our structures nor our primary data rule out the possibility that alternate side chain conformations exist in fast exchange with the predominant species described here.

Implications for BNIP3 Folding in Vivo and in Vitro. BNIP3 is a tail-anchored (TA) protein whose C-terminal transmembrane domain targets the full-length protein to mitochondrial membranes in vivo (*64*). Recent studies have identified proteins that help deliver certain TA proteins exclusively to the endoplasmic reticulum (*65*), but mitochondrial proteins bearing C-terminal TMDs of moderate hydrophobicity and flanking charged residues are ignored by the ER targeting machinery and may self-insert post-translationally into membranes of appropriate lipid composition that face the cytosol (*66*). If BNIP3 independently inserts its TMD into membranes, then the balance of charged, polar, and hydrophobic residues in the TMD should be an important determinant of this self-insertion (*67*, *68*). Our previous mutagenesis results and FTIR hydrogen exchange data indicate that noninterfacial substitutions that decrease the hydrophobicity of the TMD disrupt dimerization by altering the propensity of the peptide to fold as a helix into micelles (*30*). This suggests that the BNIP3 TMD is just sufficiently hydrophobic to partition into micelles, and that it may be similarly poised to partition into membranes. The ionizable imidazole group within the BNIP3 TMD could serve to modulate association with (and insertion across) membranes, which has been shown for a designed peptide (*68*).

The transmembrane histidine in the M2 channel protein of influenza virus participates in gating of that tetrameric channel, and deprotonation of this histidine facilitates binding of the drug amantadine (*18*) in the pore at the center of the tetramer (*16*). In contrast to the NMR and MD work of Arseniev and colleagues (*42*), our BNIP3 TMD structures show no evidence of a pore or channel, and although the geometry of the His 173 side chain is well-defined by NOE data, the tautomer/protonation state of the imidazole ring cannot be uniquely assigned from our chemical shift data. The Nε2H neutral tautomer would donate an intermonomer hydrogen bond to Ser 172, whereas the Nδ1H neutral tautomer would accept a hydrogen bond from Ser 172 of the opposite monomer and donate a hydrogen bond to the carbonyl oxygen of Leu 169 on its own monomer. If the imidazole of either monomer were to become protonated, it would have intra- and intermonomer hydrogen bond acceptors for Nδ1H and Nε2H, respectively, which would help lower the free energy of the protonated state. However, if the hydrogen bonding potential of the histidine were not satisfied, the peptide could also unfold locally and partition to the surface of the micelle. Such states would likely be in slow exchange with the helical, dimeric TMD peptide. Although generating such states is undesirable when the goal is to determine the structure of the TMD dimer, these conformations could provide insight into the folding pathway by which relatively hydrophobic sequences go from an aqueous state to a transmembrane topology. It may be possible to alter, by design, the hydrophobicity of the noninterfacial BNIP3 TMD residues to perturb the folding and insertion of the TMD without affecting its ability to dimerize once inserted across membranes. If dimerization of the inserted TMD peptide serves to pull the folding reaction forward by mass action, it may be useful to decrease the dimerization propensity to populate more strongly the monomeric or interfacial peptide states. Analyzing the effects of such changes could help elucidate the in vivo and in vitro folding pathways of BNIP3, and possibly mitochondrially targeted TA proteins in general. Understanding the physical basis for the effects of such mutations could lead to better approaches to solubilizing membrane peptides and proteins for structural and biochemical analysis.

ACKNOWLEDGMENT

We thank members of the Shamoo and MacKenzie laboratories for helpful discussions and suggestions, Sean Moran for maintenance of the Rice Bio-NMR Facility and technical assistance with the spectrometers, and R. Blake Hill for critical evaluation of the manuscript. The Gulf Coast Consortium 800 MHz NMR spectrometer at Rice University was made possible by a donation from the John S. Dunn, Sr., Research Foundation. The carbon-enhanced HCN cold probe on the Varian Inova 600 MHz NMR spectrometer at Rice University was obtained through SPRING (Strategic Partnership for Research in Nanotechnology) Grant AFRL (AFOSR) FA9550-04-1-0328.

SUPPORTING INFORMATION AVAILABLE

Three supplemental figures mentioned in the text: details of 2D $^{1}H-^{15}N$ HSQC spectra of lipid titrations, 2D $^{1}H-^{13}C$ HSQC spectra of samples with 10 mM DPPC or 10 mM DPPA, and bar graphs of CSI scores for individual nuclei. This material is available free of charge via the Internet at http://pubs.acs.org.

REFERENCES

1. MacKenzie, K. R. (2006) Folding and Stability of α-Helical Integral Membrane Proteins. *Chem. Rev. 106*, 1931–1977.
2. MacKenzie, K. R., Prestegard, J. H., and Engelman, D. M. (1997) A transmembrane helix dimer: Structure and implications. *Science 276*, 131–133.
3. Chamberlain, A. K., and Bowie, J. U. (2004) Analysis of side-chain rotamers in transmembrane proteins. *Biophys. J. 87*, 3460–3469.
4. Popot, J. L., and Engelman, D. M. (1990) Membrane protein folding and oligomerization: The two-stage model. *Biochemistry 29*, 4031–4037.
5. Lemmon, M. A., Treutlein, H. R., Adams, P. D., Brunger, A. T., and Engelman, D. M. (1994) A dimerization motif for transmembrane α-helices. *Nat. Struct. Biol. 1*, 157–163.
6. Lemmon, M. A., Flanagan, J. M., Treutlein, H. R., Zhang, J., and Engelman, D. M. (1992) Sequence specificity in the dimerization of transmembrane α-helices. *Biochemistry 31*, 12719–12725.
7. MacKenzie, K. R., and Engelman, D. M. (1998) Structure-based prediction of the stability of transmembrane helix-helix interactions: The sequence dependence of glycophorin A dimerization. *Proc. Natl. Acad. Sci. U.S.A. 95*, 3583–3590.
8. Doura, A. K., and Fleming, K. G. (2004) Complex interactions at the helix-helix interface stabilize the glycophorin A transmembrane dimer. *J. Mol. Biol. 343*, 1487–1497.
9. Doura, A. K., Kobus, F. J., Dubrovsky, L., Hibbard, E., and Fleming, K. G. (2004) Sequence context modulates the stability of a GxxxG-mediated transmembrane helix-helix dimer. *J. Mol. Biol. 341*, 991–998.
10. Fleming, K. G., and Engelman, D. M. (2001) Specificity in transmembrane helix-helix interactions can define a hierarchy of stability for sequence variants. *Proc. Natl. Acad. Sci. U.S.A. 98*, 14340–14344.
11. Duong, M. T., Jaszewski, T. M., Fleming, K. G., and MacKenzie, K. R. (2007) Changes in apparent free energy of helix-helix dimerization

in a biological membrane due to point mutations. *J. Mol. Biol. 371*, 422–434.
12. Smith, S. O., Eilers, M., Song, D., Crocker, E., Ying, W., Groesbeek, M., Metz, G., Ziliox, M., and Aimoto, S. (2002) Implications of threonine hydrogen bonding in the glycophorin A transmembrane helix dimer. *Biophys. J. 82*, 2476–2486.
13. Riley, M. L., Wallace, B. A., Flitsch, S. L., and Booth, P. J. (1997) Slow α helix formation during folding of a membrane protein. *Biochemistry 36*, 192–196.
14. Meindl-Beinker, N. M., Lundin, C., Nilsson, I., White, S. H., and von Heijne, G. (2006) Asn- and Asp-mediated interactions between transmembrane helices during translocon-mediated membrane protein assembly. *EMBO Rep. 7*, 1111–1116.
15. Schnell, J. R., and Chou, J. J. (2008) Structure and mechanism of the M2 proton channel of influenza A virus. *Nature 451*, 591–595.
16. Stouffer, A. L., Acharya, R., Salom, D., Levine, A. S., Di Costanzo, L., Soto, C. S., Tereshko, V., Nanda, V., Stayrook, S., and DeGrado, W. F. (2008) Structural basis for the function and inhibition of an influenza virus proton channel. *Nature 451*, 596–599.
17. Duong-Ly, K. C., Nanda, V., Degrado, W. F., and Howard, K. P. (2005) The conformation of the pore region of the M2 proton channel depends on lipid bilayer environment. *Protein Sci. 14*, 856–861.
18. Salom, D., Hill, B. R., Lear, J. D., and DeGrado, W. F. (2000) pH-dependent tetramerization and amantadine binding of the transmembrane helix of M2 from the influenza A virus. *Biochemistry 39*, 14160–14170.
19. Nguyen, P. A., Soto, C. S., Polishchuk, A., Caputo, G. A., Tatko, C. D., Ma, C., Ohigashi, Y., Pinto, L. H., Degrado, W. F., and Howard, K. P. (2008) pH-Induced Conformational Change of the Influenza M2 Protein C-Terminal Domain. *Biochemistry 47*, 9934–9936.
20. Stouffer, A. L., Nanda, V., Lear, J. D., and DeGrado, W. F. (2005) Sequence determinants of a transmembrane proton channel: An inverse relationship between stability and function. *J. Mol. Biol. 347*, 169–179.
21. Stouffer, A. L., Ma, C., Cristian, L., Ohigashi, Y., Lamb, R. A., Lear, J. D., Pinto, L. H., and DeGrado, W. F. (2008) The interplay of functional tuning, drug resistance, and thermodynamic stability in the evolution of the M2 proton channel from the influenza A virus. *Structure 16*, 1067–1076.
22. Call, M. E., Schnell, J. R., Xu, C., Lutz, R. A., Chou, J. J., and Wucherpfennig, K. W. (2006) The structure of the zetazeta transmembrane dimer reveals features essential for its assembly with the T cell receptor. *Cell 127*, 355–368.
23. Oxenoid, K., and Chou, J. J. (2005) The structure of phospholamban pentamer reveals a channel-like architecture in membranes. *Proc. Natl. Acad. Sci. U.S.A. 102*, 10870–10875.
24. Bocharov, E. V., Mineev, K. S., Volynsky, P. E., Ermolyuk, Y. S., Tkach, E. N., Sobol, A. G., Chupin, V. V., Kirpichnikov, M. P., Efremov, R. G., and Arseniev, A. S. (2008) Spatial structure of the dimeric transmembrane domain of the growth factor receptor ErbB2 presumably corresponding to the receptor active state. *J. Biol. Chem. 283*, 6950–6956.
25. MacKenzie, K. R., and Fleming, K. G. (2008) Association energetics of membrane spanning α-helices. *Curr. Opin. Struct. Biol. 18*, 412–419.
26. Yin, H., Slusky, J. S., Berger, B. W., Walters, R. S., Vilaire, G., Litvinov, R. I., Lear, J. D., Caputo, G. A., Bennett, J. S., and DeGrado, W. F. (2007) Computational design of peptides that target transmembrane helices. *Science 315*, 1817–1822.
27. Bruick, R. K. (2000) Expression of the gene encoding the proapoptotic Nip3 protein is induced by hypoxia. *Proc. Natl. Acad. Sci. U.S.A. 97*, 9082–9087.
28. Lee, H., and Paik, S. G. (2006) Regulation of BNIP3 in normal and cancer cells. *Mol. Cells 21*, 1–6.
29. Sulistijo, E. S., Jaszewski, T. M., and MacKenzie, K. R. (2003) Sequence-specific dimerization of the transmembrane domain of the "BH3-only" protein BNIP3 in membranes and detergent. *J. Biol. Chem. 278*, 51950–51956.
30. Sulistijo, E. S., and MacKenzie, K. R. (2006) Sequence Dependence of BNIP3 Transmembrane Domain Dimerization Implicates Side-chain Hydrogen Bonding and a Tandem GxxxG Motif in Specific Helix-Helix Interactions. *J. Mol. Biol. 364*, 974–990.
31. Kim, S., Jeon, T. J., Oberai, A., Yang, D., Schmidt, J. J., and Bowie, J. U. (2005) Transmembrane glycine zippers: Physiological and pathological roles in membrane proteins. *Proc. Natl. Acad. Sci. U.S.A. 102*, 14278–14283.
32. Ben-Tal, N., and Honig, B. (1996) Helix-helix interactions in lipid bilayers. *Biophys. J. 71*, 3046–3050.
33. White, S. H., and Wimley, W. C. (1999) Membrane protein folding and stability: Physical principles. *Annu. Rev. Biophys. Biomol. Struct. 28*, 319–365.
34. Jayasinghe, S., Hristova, K., and White, S. H. (2001) Energetics, stability, and prediction of transmembrane helices. *J. Mol. Biol. 312*, 927–934.
35. White, S. H. (2005) How hydrogen bonds shape membrane protein structure. *Adv. Protein Chem. 72*, 157–172.
36. Choma, C., Gratkowski, H., Lear, J. D., and DeGrado, W. F. (2000) Asparagine-mediated self-association of a model transmembrane helix. *Nat. Struct. Biol. 7*, 161–166.
37. Zhou, F. X., Cocco, M. J., Russ, W. P., Brunger, A. T., and Engelman, D. M. (2000) Interhelical hydrogen bonding drives strong interactions in membrane proteins. *Nat. Struct. Biol. 7*, 154–160.
38. Gratkowski, H., Lear, J. D., and DeGrado, W. F. (2001) Polar side chains drive the association of model transmembrane peptides. *Proc. Natl. Acad. Sci. U.S.A. 98*, 880–885.
39. Stanley, A. M., and Fleming, K. G. (2007) The role of a hydrogen bonding network in the transmembrane β-barrel OMPLA. *J. Mol. Biol. 370*, 912–924.
40. Joh, N. H., Min, A., Faham, S., Whitelegge, J. P., Yang, D., Woods, V. L., and Bowie, J. U. (2008) Modest stabilization by most hydrogen-bonded side-chain interactions in membrane proteins. *Nature 453*, 1266–1270.
41. Metcalf, D. G., Law, P. B., and DeGrado, W. F. (2007) Mutagenesis data in the automated prediction of transmembrane helix dimers. *Proteins 67*, 375–384.
42. Bocharov, E. V., Pustovalova, Y. E., Pavlov, K. V., Volynsky, P. E., Goncharuk, M. V., Ermolyuk, Y. S., Karpunin, D. V., Schulga, A. A., Kirpichnikov, M. P., Efremov, R. G., Maslennikov, I. V., and Arseniev, A. S. (2007) Unique dimeric structure of BNip3 transmembrane domain suggests membrane permeabilization as a cell death trigger. *J. Biol. Chem. 282*, 16256–16266.
43. Lemmon, M. A., Flanagan, J. M., Hunt, J. F., Adair, B. D., Bormann, B. J., Dempsey, C. E., and Engelman, D. M. (1992) Glycophorin A dimerization is driven by specific interactions between transmembrane α-helices. *J. Biol. Chem. 267*, 7683–7689.
44. Zwahlen, C., Legault, P., Vincent, S. J. F., Greenblatt, J., Konrat, R., and Kay, L. E. (1997) Methods for Measurement of Intermolecular NOEs by Multinuclear NMR Spectroscopy: Application to a Bacteriophage λ N-Peptide/*boxB* RNA Complex. *J. Am. Chem. Soc. 119*, 6711–6721.
45. Bax, A., Vuister, G. W., Grzesiek, S., Delaglio, F., Wang, A. C., Tschudin, R., and Zhu, G. (1994) Measurement of homo- and heteronuclear J couplings from quantitative J correlation. *Methods Enzymol. 239*, 79–105.
46. MacKenzie, K. R., Prestegard, J. H., and Engelman, D. M. (1996) Leucine side-chain rotamers in a glycophorin A transmembrane peptide as revealed by three-bond carbon-carbon couplings and ^{13}C chemical shifts. *J. Biomol. NMR 7*, 256–260.
47. Delaglio, F., Grzesiek, S., Vuister, G. W., Zhu, G., Pfeifer, J., and Bax, A. (1995) NMRPipe: A multidimensional spectral processing system based on UNIX pipes. *J. Biomol. NMR 6*, 277–293.
48. Yamazaki, T., Forman-Kay, J. D., and Kay, L. E. (1993) Two-dimensional NMR experiments for correlating carbon-13 β and proton δ/ε chemical shifts of aromatic residues in ^{13}C-labeled proteins via scalar couplings. *J. Am. Chem. Soc. 115*, 11054–11055.
49. Linge, J. P., Habeck, M., Rieping, W., and Nilges, M. (2003) ARIA: Automated NOE assignment and NMR structure calculation. *Bioinformatics 19*, 315–316.
50. Brunger, A. T., Adams, P. D., Clore, G. M., DeLano, W. L., Gros, P., Grosse-Kunstleve, R. W., Jiang, J. S., Kuszewski, J., Nilges, M., Pannu, N. S., Read, R. J., Rice, L. M., Simonson, T., and Warren, G. L. (1998) Crystallography & NMR system: A new software suite for macromolecular structure determination. *Acta Crystallogr. D54*, 905–921.
51. Laskowski, R. A., Rullmannn, J. A., MacArthur, M. W., Kaptein, R., and Thornton, J. M. (1996) AQUA and PROCHECK-NMR: Programs for checking the quality of protein structures solved by NMR. *J. Biomol. NMR 8*, 477–486.
52. Pelton, J. G., Torchia, D. A., Meadow, N. D., and Roseman, S. (1993) Tautomeric states of the active-site histidines of phosphorylated and unphosphorylated IIIGlc, a signal-transducing protein from *Escherichia coli*, using two-dimensional heteronuclear NMR techniques. *Protein Sci. 2*, 543–558.
53. Hass, M. A., Hansen, D. F., Christensen, H. E., Led, J. J., and Kay, L. E. (2008) Characterization of conformational exchange of a histidine side chain: Protonation, rotamerization, and tautomerization of

His61 in plastocyanin from *Anabaena variabilis*. *J. Am. Chem. Soc. 130*, 8460–8470.
54. Wishart, D. S., and Case, D. A. (2001) Use of chemical shifts in macromolecular structure determination. *Methods Enzymol. 338*, 3–34.
55. Senes, A., Ubarretxena-Belandia, I., and Engelman, D. M. (2001) The Cα−H···O hydrogen bond: A determinant of stability and specificity in transmembrane helix interactions. *Proc. Natl. Acad. Sci. U.S.A. 98*, 9056–9061.
56. Vargas, R., Garza, J., Dixon, D. A., and Hay, B. P. (2000) How Strong Is the Cα−H···O═C Hydrogen Bond?. *J. Am. Chem. Soc. 122*, 4750–4755.
57. Mottamal, M., and Lazaridis, T. (2005) The contribution of Cα−H···O hydrogen bonds to membrane protein stability depends on the position of the amide. *Biochemistry 44*, 1607–1613.
58. Dunbrack, R. L.Jr. (2002) Rotamer libraries in the 21st century. *Curr. Opin. Struct. Biol. 12*, 431–440.
59. Lifshitz, Y., Petrovich, E., Haviv, H., Goldshleger, R., Tal, D. M., Garty, H., and Karlish, S. J. (2007) Purification of the human α2 Isoform of Na,K-ATPase expressed in *Pichia pastoris*. Stabilization by lipids and FXYD1. *Biochemistry 46*, 14937–14950.
60. Ahn, T., Yun, C. H., and Oh, D. B. (2005) Involvement of non-lamellar-prone lipids in the stability increase of human cytochrome P450 1A2 in reconstituted membranes. *Biochemistry 44*, 9188–9196.
61. Molina, M. L., Encinar, J. A., Barrera, F. N., Fernandez-Ballester, G., Riquelme, G., and Gonzalez-Ros, J. M. (2004) Influence of C-terminal protein domains and protein-lipid interactions on tetramerization and stability of the potassium channel KcsA. *Biochemistry 43*, 14924–14931.
62. Marsh, D. (2008) Protein modulation of lipids, and vice-versa, in membranes. *Biochim. Biophys. Acta 1778*, 1545–1575.
63. Tian, C., Karra, M. D., Ellis, C. D., Jacob, J., Oxenoid, K., Sonnichsen, F., and Sanders, C. R. (2005) Membrane protein preparation for TROSY NMR screening. *Methods Enzymol. 394*, 321–334.
64. Yasuda, M., Theodorakis, P., Subramanian, T., and Chinnadurai, G. (1998) Adenovirus E1B-19K/BCL-2 interacting protein BNIP3 contains a BH3 domain and a mitochondrial targeting sequence. *J. Biol. Chem. 273*, 12415–12421.
65. Stefanovic, S., and Hegde, R. S. (2007) Identification of a targeting factor for posttranslational membrane protein insertion into the ER. *Cell 128*, 1147–1159.
66. Borgese, N., Brambillasca, S., and Colombo, S. (2007) How tails guide tail-anchored proteins to their destinations. *Curr. Opin. Cell Biol. 19*, 368–375.
67. Ladokhin, A. S., and White, S. H. (2001) Protein chemistry at membrane interfaces: Non-additivity of electrostatic and hydrophobic interactions. *J. Mol. Biol. 309*, 543–552.
68. Ladokhin, A. S., and White, S. H. (2004) Interfacial folding and membrane insertion of a designed helical peptide. *Biochemistry 43*, 5782–5791.
69. Derewenda, Z. S., Lee, L., and Derewenda, U. (1995) The occurrence of C−H···O hydrogen bonds in proteins. *J. Mol. Biol. 252*, 248–262.